# Characterization of a Fiber-Optic Evanescent Wave Absorbance Sensor for Nonpolar Organic Compounds

## J.-P. CONZEN, J. BÜRCK,* and H.-J. ACHE
*Kernforschungszentrum Karlsruhe, Institut für Radiochemie, Postfach 3640, D-7500 Karlsruhe 1, Germany*

A fiber-optic evanescent field absorbance sensor (EFAS) is described, for which the sensing element consists of a commercially available silicone-clad quartz glass fiber, coiled on a Teflon® support. The polydimethylsiloxane cladding fulfills various functions. It protects the brittle fiber core against fracture induced by mechanical stress. Moreover, as a lower-refractive-index medium, it causes total reflection in the fiber and acts as a hydrophobic membrane that enriches nonpolar organic compounds, whereas polar species like water cannot penetrate. Coupled to an NIR spectrometer, the sensor has a potential for remote *in situ* measurements of organic pollutants in drainage waters originating from contaminated areas. In this study aqueous solutions of typical drainage-water contaminants like dichloromethane, chloroform, and trichloroethylene were measured in the 900–2100 nm spectral range. The influence of refractive index, fiber length and diameter, bend radius, polysiloxane swelling, and ambient temperature on the sensor signal is described and qualitatively compared with theoretical predictions. Kinetics measurements are presented, which allow explanation of the diffusion mechanism of $CHCl_3$ enrichment in the polysiloxane cladding. The data show that the rate-determining step for penetration of this substance into the sensor polymer layer can be described mainly by film diffusion through the aqueous boundary layer. In most cases no remarkable influence of gel diffusion in the polysiloxane membrane was observed.

Index Headings: Evanescent wave; Sensor; Fiber optics; NIR; Chlorinated hydrocarbons; Kinetics.

## INTRODUCTION

Chlorinated hydrocarbon solvents (CHS) have often been used in chemical and industrial processes. For example, dichloromethane and trichloroethylene have been applied as solvents in the production of lacquers or as degreasing agents on metal surfaces; chloroform has been used as starting material in the production of refrigerants.[1] Large amounts of these substances have been spilled in the environment and have contaminated soil and ground waters. Therefore, considerable effort is directed today towards developing continuous measurement techniques for a long-term control of effluents from contaminated areas, or for the surveillance of decontamination procedures.

A promising answer to such demands seems to be fiber-optic chemical sensor systems (FOCS).[2,3] Among other concepts, FOCS can be built by using the evanescent wave principle, which was discovered by Goos and Hänchen.[4] If a light beam is directed into a glass fiber, which is surrounded by a medium of lower refractive index (RI), a part of the beam will be transmitted by total internal reflection at the core/cladding interface. The resulting standing wave will penetrate over a small distance into the lower RI medium where it can interact

with molecules. Due to this process, the medium of lower refractive index will absorb energy from the evanescent field at frequencies specific to the respective substance. The sensitivity of the method can be increased by using a fiber length of several meters along which the light is reflected many times.

Several approaches based on the evanescent wave principle have been described in the literature. Among the first were the optode-type approaches, according to which a dye or a fluorescent indicator is immobilized at the tip of an optical fiber.[5,6] In this case there is only one point of internal reflection where the light beam can interact with an analyte. In later applications, a fiber core was used as an internal reflection element directly surrounded by the analyte medium, which resulted in a higher number of points of reflection.[7] To be able to measure nonpolar organic species, a still better approach consists of using a quartz glass core coated with a low-RI polymer membrane.[8] Moreover, with this design of an "extracting" membrane it is possible to enrich nonpolar compounds, whereas polar species like water are excluded.[9] Hence, when measuring aqueous solutions of, e.g., chlorinated hydrocarbons, one has the particular advantage of avoiding interferences from strong water OH-absorption bands. Compared to those for conventional NIR spectroscopy in quartz glass cuvettes, the limits of detection are decreased in this way at least by a factor of 100–1000, and most CHSs can be measured down to the low-ppm range.

Cladding materials which exhibit the most suitable properties for evanescent wave FOCS are of the polyalkylsiloxane type $(RR'-Si-O-)_n$. For instance, the dielectric constant $\epsilon_r$ of polydimethylsiloxane is very low compared to that of water $[\epsilon_r(H_2O) = 78]$ and varies as a function of the molecular weight from 2.63 to 2.77.[10] This is a value which is in the same range as the dielectric constants of most chlorinated hydrocarbons.[11] Therefore, a good interaction between these nonpolar species and the polymer cladding can be predicted, which leads to high distribution coefficients in the silicone/water system. Moreover, due to their low RI, good spectral transmission in the NIR range, and high chemical and mechanical stability, these materials are preferably used to coat quartz glass fiber cores.

The surveillance of CHS decontamination procedures, on the other hand, requires short response times of the detecting system in order to reach a near-real-time process control. Hence, a fast transport of the hydrophobic molecules through the polymer membrane to the cladding/core interface of the fiber is essential. One important aspect when creating an EFAS sensing element is therefore to understand the kinetic behavior of the sen-

sor/analyte system. In this context, polydialkylsiloxanes are also considered to be among the favorable cladding materials. The high diffusion coefficients of nonpolar organic substances in this polymer type provide a means of building fast detecting sensors.

## THEORY

**Evanescent Wave Spectroscopy.** A light beam which is incident on the core/cladding interface of a glass fiber is partially reflected and partially refracted into the less dense optical medium, if the angle of incidence $\theta$ is smaller than the critical angle $\theta_c$. With an increase in $\theta$, the portion of reflected light is raised, and, if the angle of incidence exceeds the critical angle, total internal reflection occurs. Equation 1, which is easily obtained from Snell's law with an angle of refraction equal to 90°, shows that the critical angle $\theta_c$ depends only on the refractive indices $n_1$ and $n_2$ of the core and cladding materials, respectively:

$$\sin \theta_c = n_2/n_1. \tag{1}$$

There are no transmission losses during light propagation except for the intrinsic absorption of the fiber material. The refractive index of the cladding $n_2$ has to be smaller than $n_1$, and, if the difference between the refractive indices is increased, $\theta_c$ will decrease and more light will be transported. There is a standing wave at every point of total internal reflection at the core/cladding interface. This harmonic wave, which penetrates over a small distance into the surrounding medium, is called the evanescent wave and can be described by the exponential decay

$$E = E_0 \cdot \exp(-z/d_p) \tag{2}$$

where $z$ is the distance normal to the interface and $E_0$ is the wave amplitude at $z = 0$. The penetration depth is given by

$$d_p = \lambda/(n_1 \cdot 2\pi)(\sin^2\theta - (n_2/n_1)^2)^{0.5} \tag{3}$$

where $\lambda$ is the wavelength of light in the fiber core.[12]

From Eq. 3 it can be seen that for small differences between $n_1$ and $n_2$ the penetration depth is increased and more light energy becomes available for interaction with the external medium. Simultaneously, less light can be transported through the fiber core due to the increase in critical angle (if the ratio of $n_2$ to $n_1$ approaches unity, the penetration depth becomes infinite and no light is reflected).

Fiber-optic evanescent field absorbance measurements are performed by comparing the light intensity of a sensor immersed in the analyte solution to the intensity of the sensor in air or in pure water. If an organic compound is enriched in the cladding, the RI of the CHS loaded polymer will change. At a nonabsorbing wavelength, this will cause a change in numerical aperture (NA), according to the change in critical angle for total internal reflection, and the resulting absorbance signal is given by:[13]

$$-\log(I/I_0) = \log \text{NA}_0^2/\text{NA}^2 \tag{4}$$
$$\text{NA}_0 = (n_1^2 - n_2^2)^{1/2} \tag{5}$$
$$\text{NA} = (n_1^2 - n^2)^{1/2} \tag{6}$$

where $I$ is the transmitted light intensity of the sensor immersed in the analyte solution, $I_0$ is the transmitted light intensity when the sensor is in air or in pure water, and $n$ is the refractive index of the solvent-loaded cladding.

At an absorbing wavelength, the spectrum provides absorbance and refractive index information, and both parameters depend on each other. On the one hand, the RI of the cladding influences the penetration depth of the field intensity (cf. Eq. 3) and, on the other hand, the RI is connected to the absorptivity coefficient at an absorbing wavelength.[14] According to both effects, the signal of an evanescent wave sensor at an absorbing wavelength is given by

$$-\log(I/I_0) = \alpha_e \cdot l \cdot c + \log(\text{NA}_0^2/\text{NA}^2) \tag{7}$$

where $\alpha_e = \eta_p \cdot \epsilon$ is the effective absorptivity, $\epsilon$ is the molar absorptivity, $l$ is the fiber length, and $c$ is the analyte concentration.[15] The power distribution, which can be calculated from

$$\eta_p = k \cdot \lambda/2\pi \cdot r \cdot \text{NA} \tag{8}$$

is given by the ratio of light energy in the evanescent field to the total light intensity transported in the fiber core; $k$ is a constant and $r$ is the fiber radius.[16]

The first term of Eq. 7 describes the attenuation caused by the light absorption in the cladding material and shows a pseudo-Beer's-dependence of the absorbance on the fiber length and the analyte concentration. However, a large effect of the cladding RI on the effective absorptivity $\alpha_e$ can be observed, which is correlated to the power distribution $\eta_p$. At identical wavelengths for fibers of the same radius, the power distribution depends on the numerical aperture (cf. Eq. 8). Due to analyte enrichment in the cladding, the concomitant variation in the cladding RI leads to a change of the effective absorptivity. This influence has been calculated for different changes in the refractive index. In Fig. 1 the effective absorptivity, normalized to the value of the undiluted cladding (RI = 1.436), is plotted against the presumed refractive index. It can be seen that a change in RI of the surrounding medium (cladding plus analyte) leads to a nonlinear change in the effective absorptivity and, consequently, also in the resulting absorbance values (cf. first term in Eq. 7). If the RI is increased due to analyte enrichment, $\alpha_e$ grows rapidly and becomes infinite if the refractive index of the core (RI = 1.456) is reached. With a decrease in the RI the effective absorptivity is diminished, which results in a lower absorbance signal. In each case a positive deviation from linearity can be predicted.

The influence of the cladding RI on the second term of Eq. 7, which describes the refraction effects (cf. Eq. 4), can be discussed in a similar way. The calculated absorbance values, which contribute as a summand to the total absorbance, are shown in Fig. 2. Again positive deviations from linearity are observed if the values are plotted against the RI of the surrounding medium.

Temperature and polymer-swelling effects can also influence the fiber NA. The cladding is expanded by an increase in temperature or by the enrichment of an analyte. The result is a decrease of the cladding RI, and the corresponding sensor absorbance values will be diminished.
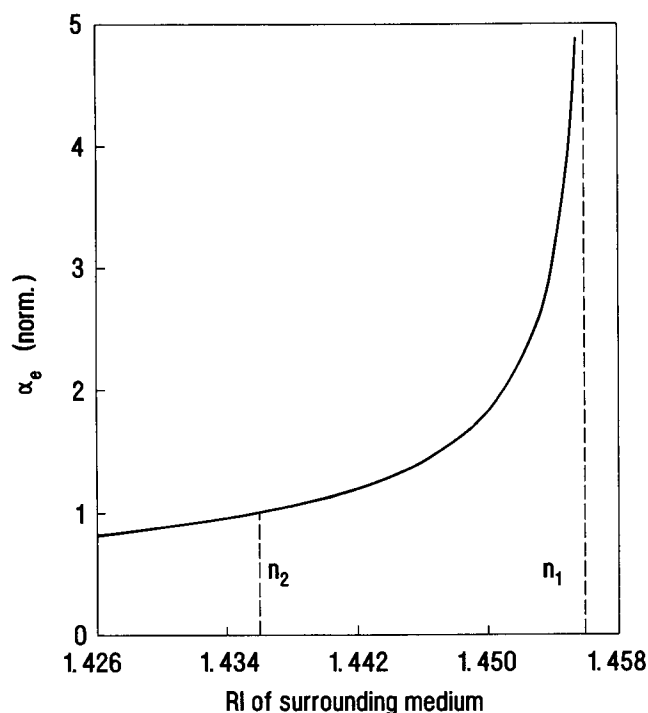
FIG. 1. Calculated normalized effective absorptivity $\alpha_e$ vs. refractive index of the surrounding medium (cladding plus analyte).



FIG. 2. Calculated contribution of the refraction term of Eq. 7 to the sensor response.

At this point it is important to notice that Eq. 7 does not give a complete theoretical description of the absorbance spectrum obtained by an evanescent wave sensor. It observes only the totally reflected part of the light in an unbent fiber and assumes equal field intensities in all optical modes. Bending of the fiber leads to a destruction of the axial symmetry that has been assumed so far. With a smaller bend radius, light propagation is shifted, on the one hand, to higher modes[17] that have a higher penetration depth in the cladding. On the other hand, due to an increased critical angle more light is coupled out, resulting in a lower total intensity of light transmitted through the fiber. With the use of the formula of Takeo and Hattori,[18] this influence has been calculated for several ratios of bend radius $R$ and fiber diameter $d$ of the fiber used in our experiments. From the data given in Table I it can be seen that the total reflection area of the fiber cross section decreases drastically with lower-bend radii.

Moreover, the refractive index at an absorbing wavelength becomes a complex variable due to the fact that the interaction of radiation and molecules causes an energy transfer to the molecules. Besides the real part of the dispersion curve, an increasingly higher imaginary part will be found by approaching an absorbing wavelength.[19] As mentioned above, the sensor response signal depends heavily on the RI, and this effect of anomolous dispersion adds another difficulty to finding a quantitative theoretical description of the absorbance values.

Nevertheless, one can estimate from Eq. 7 that the absorbance values will increase with higher absorptivity and concentrations of the analyte as well as with greater fiber lengths, longer wavelengths, smaller fiber radii, and smaller differences between the refractive index of the core and the cladding material.
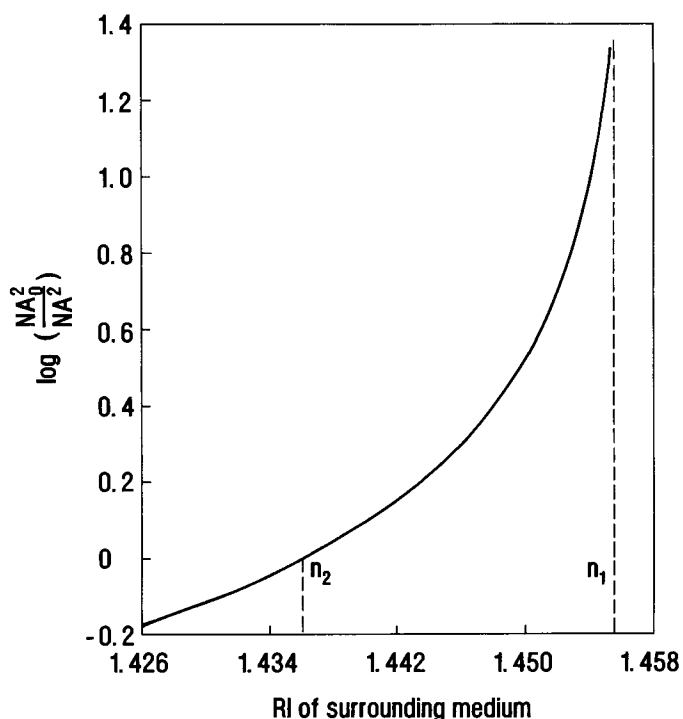
**Kinetics and Diffusion.** In view of minimizing the response times of polymer-coated evanescent wave FOCSs, it is important to understand the mechanism of analyte diffusion into the sensor membrane. In general, two steps appear to be rate controlling: the molecule movement in the aqueous solution and that in the polysiloxane bulk.

If molecule movement in the aqueous solution is the rate-determining step, the model of Nernst has to be taken into consideration. This is illustrated in Fig. 3, where the concentration and the velocity profile of the analyte molecules at the sensor surface are shown. Before the sensor is immersed in the solution, a homogeneous analyte concentration can be assumed. After immersion, the concentration at the water/polymer interface will decrease due to analyte enrichment in the cladding. In this case, molecule movement in the polymer bulk is supposed to be faster than in the aqueous solution. Hence, after a short initial delay, the concentration of the analyte at the surface of the sensor reaches a constant lower value. By approaching the solid surface, the resulting real concentration profile in the aqueous phase is given by a continuous decrease. The model of Nernst approximates this profile by a film of defined thickness where the concentration decreases linearly and the molecules are moved only by diffusion.

TABLE I. Fraction of fiber cross section A, which transmits light by total reflection.

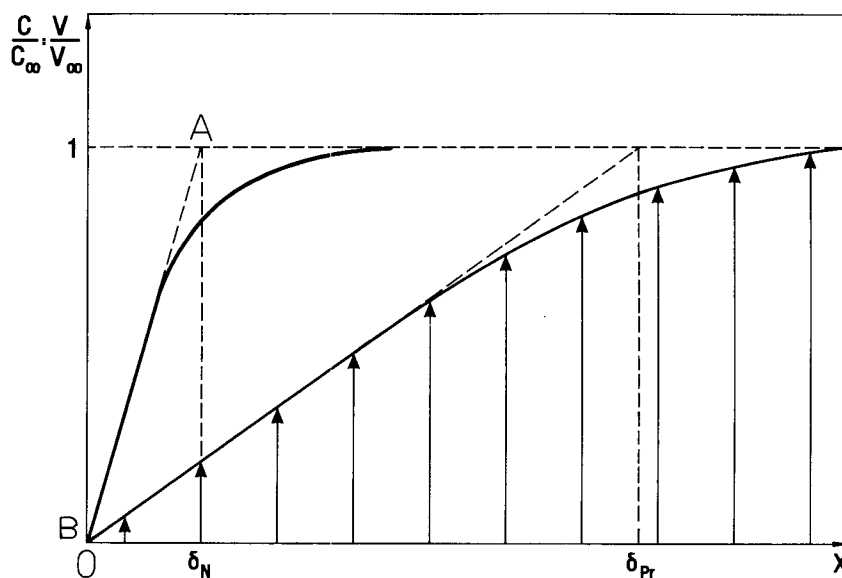| $R : d$ | A (%) |
|---|---|
| 120:1 | 83.2 |
| 60:1 | 56.1 |
| 30:1 | 28.5 |
| 10:1 | 10.1 |
| 5:1 | 5.5 |
| 2:1 | 2.8 |

FIG. 3. Normalized concentration and velocity profile in a laminar flow at the sensor surface.

This zone is generally called the Nernstian boundary layer $\delta_N$ (NBL). In unstirred solutions, the film of varying concentration grows permanently into the bulk of the aqueous solution. The concentration gradient which determines the flux of molecules through the layer levels off. In stirred solutions, the thickness of the NBL is constant and only a function of the hydrodynamic behavior of the liquid medium.[20]

In a similar way, the velocity gradient of the molecules in the space surrounding the sensor surface can be simplified by a zone of defined thickness in which no convection occurs and a linear decrease in the velocity of the molecules is assumed. This zone is called Prandtl layer $\delta_{Pr}$ and can be correlated to the Nernstian boundary layer:[20]

$$\delta_N = \delta_{Pr} \cdot Pr^{-1/3} \qquad (9)$$

where Pr is the Prandtl number. This dimensionless group compares the momentum transport with the energy transport in the liquid. It is generally given by:

$$Pr = \nu/D \qquad (10)$$

where $\nu$ is the kinematic viscosity of the solution, and $D$ is the diffusion coefficient of the analyte. For aqueous solutions $\nu$ is on the order of $10^{-2}$ cm$^2$s$^{-1}$ and $D$ is on the order of $10^{-5}$ cm$^2$s$^{-1}$, resulting in a Prandtl number of 1000.[20] According to Eqs. 9 and 10, the thickness of the Nernstian boundary layer is given by

$$\delta_N = 0.1 \cdot \delta_{Pr}. \qquad (11)$$

Hence, for analytes in aqueous solutions, the thickness of the Nernstian boundary layer is only 10% of the thickness of the Prandtl boundary layer.

For analyte movement in the sensor cladding, the structural behavior of the silicone polymer has to be taken into consideration. Normally, diffusion coefficients for molecule movement in dilute aqueous solution are on the order of $10^{-5}$ cm$^2$s$^{-1}$ (see Ref. 21), and for movement in a polymer bulk in the $10^{-8}$–$10^{-9}$ cm$^2$s$^{-1}$ range.[22] However, the physical behavior of the cladding material can-

not be described by solid-state properties. Due to its structure, polydimethylsiloxane is one of the most flexible chain molecules known today, which can be seen by looking at its glass temperature of $-125°C$, which is lower than that for all other polymers.[23] On the one hand, the Si-O-bond is longer (0.164 nm) and the Si-O-Si-angle (143°) much more open than for comparable organic polymers (length of a C-C-bond: 0.153 nm; angle of a C-C-C-bond: 109°).[23] On the other hand, the oxygen atoms are not substituted by side groups. As a consequence, the steric hindrance for a chain movement is diminished and, in addition, due to very weak molecular interactions, a polymer of an extremely high flexibility is formed, in which smaller species can easily move. The behavior of the cladding material can be characterized by the properties of a high viscous melt rather than of a solid polymer. Hence, for the movement of chlorinated hydrocarbons, a diffusion coefficient can be expected which is comparable to diffusion coefficients in aqueous solutions.

The time-dependent change of concentration in the NBL or in the polymer cladding is described by the second Fickian law:

$$dc/dt = D(d^2c/dx^2) \qquad (12)$$

with $c$ being the concentration of the diffusing substance, $t$ the time, and $x$ the length of path (the diffusion coefficient can be assumed as constant because all concentrations are in the low g L$^{-1}$ range so that no analyte–analyte interactions are expected, which would lead to measurable changes in $D$). In the case of a fiber optical waveguide, the geometry of the cladding and the attached interfacial film is approximately given by a long hollow cylinder. Assuming only radial diffusion, Eq. 12 can be written in cylinder coordinates:

$$dc/dt = (D/r) \cdot d(r \, dc/dr)/dr \qquad a < r < b \qquad (13)$$

where $a$ and $b$ are the inner and outer radii $r$, respectively.[24] This equation has to be solved according to the corresponding boundary conditions. In the case that diffusion in both the aqueous film and in the polymer bulk

is rate-determining, nonlinear boundary conditions at the polymer/film interface appear and no exact solution of Eq. 13 is available.[25] Nevertheless, for one system described in this paper several assumptions have been made that allow us to simplify the problem and to determine the diffusion mechanism.

Independent of the diffusion mechanism, the rate of CHS enrichment in the fiber cladding is usually characterized by the $t_{90}$ value (time needed to reach 90% of the equilibrium concentration). This parameter can be discussed in qualitative terms by looking at the analyte flux $j$ through the Nernstian boundary layer and the polymer bulk. Generally, the flux $j$ of molecules in a homogeneous medium is given by the first Fickian law, which can be deduced from Eq. 12:

$$j = -D \, dc/dx. \tag{14}$$

In the case of analyte enrichment in the fiber cladding Eq. 14 has to be solved simultaneously for diffusion in both phases, in the NBL and in the polymer. If the rate-determining step for CHS uptake consists solely in the diffusion through the aqueous boundary layer, the enrichment process can be described in a much simpler way. Again the model of Nernst can be applied, where the real CHS concentration gradient $dc/dx$ in the diffusion film is approximated by a linear gradient, whose slope is given by the slope of the real gradient at the sensor surface ($x = 0$, see Fig. 3). In this case the molecular flux $j_N$ through the Nernstian boundary layer can be expressed as follows:

$$j_N = -D(dc/dx)_{x=0} = -D \, \Delta c/\delta_N \tag{15}$$
$$\Delta c = c_\infty - c_s \tag{16}$$

with $c_\infty$ being the concentration of the analyte in the aqueous solution and $c_s$ the analyte concentration at the sensor surface.

The flux of molecules into the polymer membrane is proportional to the difference of concentrations at the boundaries of the NBL and inversely proportional to its extension. If the CHS diffusion coefficient, the extension of the NBL, and the analyte concentration at the sensor surface are assumed to be constant, the slope of the concentration gradient should be proportional to the "bulk" analyte concentration $c_\infty$ of the aqueous solution, and, consequently, the molecular flux should also be proportional to $c_\infty$. In this case, a twofold increase in analyte concentration should lead to a twofold molecular flux $j_N$. Therefore, the time periods necessary to reach the corresponding equilibrium and also the $t_{90}$ values should be constant.

## EXPERIMENTAL

PCS (plastic-clad silica) fibers of different lengths, diameters, and bend radii were coiled as a spiral on a Teflon® support of cylindrical geometry. The sizes of the sensors were 5.5·16 cm and 2.5·12 cm, respectively. One fiber with a 210-$\mu$m-outer-diameter (o.d.) low-hydroxyl-fused-silica core, a 230-$\mu$m-o.d. polysiloxane cladding, and a 270-$\mu$m-o.d. nylon coating and a second fiber with a 400-$\mu$m-o.d. core, a 500-$\mu$m-o.d. cladding, and a 600-$\mu$m-o.d. coating (Fiberguide Industries, Stirling, NJ) were used in the experiments. The coating was dissolved in

propylene glycol heated to 160°C for 10 min. The ends of the sensor fibers were fixed by crimp-and-cleave plugs (Ensign Bickford Optics Company, Avon, CT) and coupled to a Guidedwave spectrophotometer, Model 260. The modular optic design of the single-beam instrument consists of a tungsten halogen lamp, a stepping-motor-driven holographic grating with 300 lines/mm, and a germanium photodiode or a lead sulfide detector. Processing and storage functions were controlled by a Compaq Deskpro 286 PC. The whole experimental setup has been illustrated in a preceding paper.[9]

Dichloromethane, chloroform, and trichloroethylene of reagent-grade quality were used as delivered by Merck (Germany). The samples were prepared by adding a weighed amount of pure chlorinated hydrocarbon with a gas-tight HPLC syringe to 2.3 L deionized water in a thermostated double-walled glass container and mixing by a magnetic stirrer. After homogenization, the sensor was immersed and kinetics measurements were done in stirred or in unstirred solutions. In this case, only a spectral range of ±50 nm around the corresponding CHS peak was scanned at a rate of 1200 nm/min, allowing 10 spectra to be collected within one minute. The cover, sealed by a Teflon® O-ring, touched the surface of the solution to avoid degasing of the chlorinated hydrocarbons into the headspace above the surface of the liquid. The reference intensities for the EFAS measurements were taken in air at room temperature (22–24°C) or in a second thermostated container filled with pure deionized water. During the sample measurements the receptacles were thermostated with an accuracy in temperature of ±0.1°C. For the determination of temperature effects on the sensor response, the container temperature was varied between +5 and +40°C.

To determine the actual concentration of the solution by an independent method, we measured an aliquot of the solution sampled in a quartz glass cuvette by UV absorption spectrophotometry. The instrument used for the measurements in the 190–290 nm range was a Varian Cary 2400. Generally, a good agreement of the weighed amount of chlorinated hydrocarbon and the UV reference data was found, and no observable quantities of the substance were lost from the closed container during several days.

## RESULTS AND DISCUSSION

**Sensor Response.** To understand the parameters governing the sensor response on CHS species, we needed to carry out investigations concerning the influence of fiber length, diameter, and bending as well as studies of the cladding refractive index and ambient temperature.

The C-H first overtone vibration absorption bands of most organic compounds can be found in the 1600–1800 nm spectral range.[26] The EFAS absorbance spectra of three different CHSs are presented in Fig. 4. For chloroform a band appears at 1692 nm, for trichloroethylene a band appears at 1650 nm, and for dichloromethane two bands at 1650 and 1692 nm can be observed. Additional (positive or negative) absorption peaks in the spectral region from 1660 to 1780 nm are due to interferences from the silicone cladding.[9] The dependence of the EFAS absorbance on the concentration of these three com-
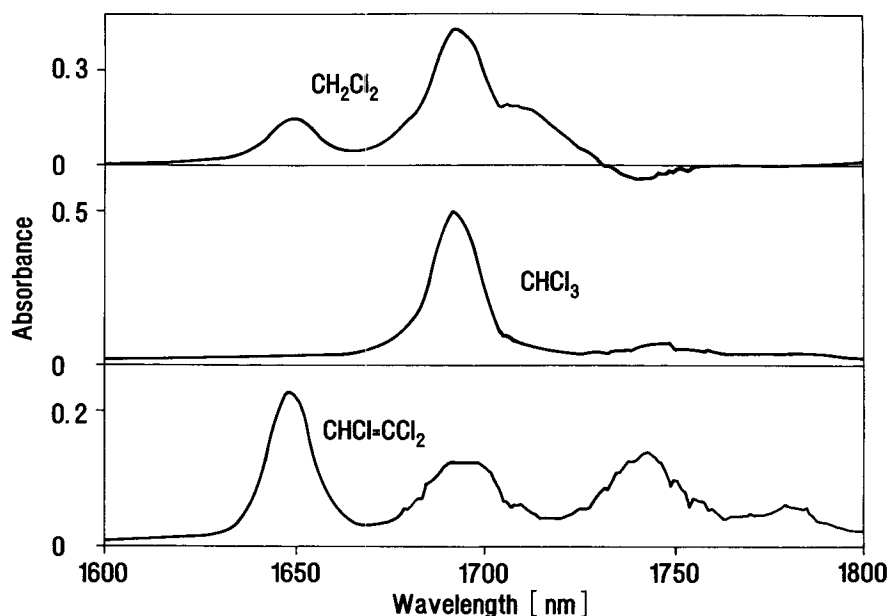
FIG. 4. Evanescent field absorption spectra of aqueous solutions of $CH_2Cl_2$ (0.188 mol $L^{-1}$), $CHCl_3$ ($3.95 \cdot 10^{-2}$ mol $L^{-1}$), and $CHCl=CCl_2$ ($4.07 \cdot 10^{-3}$ mol $L^{-1}$); 6.43-m length/500-$\mu$m-o.d. cladding/400-$\mu$m-o.d. core fiber sensor.

pounds in the aqueous solution is shown in Fig. 5. Distinct differences in the sensitivity of the absorbance signal for the three species can be observed (the sensitivity is given by the slope of the curves). Starting from the fact that the molar extinction coefficients of $CH_2Cl_2$, $CHCl_3$, and $CHCl=CCl_2$ in a nonpolar solvent are of the same order of magnitude,[27] one can conclude that this parameter should be comparable also for "solutions" of these species in a polydimethylsiloxane matrix.[28] The enormous differences in the sensitivities should then be caused by the different actual concentrations of the CHSs in the cladding due to different distributions of the molecules between the silicone and water matrix.

The distribution of a CHS between the aqueous solution and the polydimethylsiloxane matrix is a function of molecular interactions described by the distribution coefficient $K_D$:

$$K_D(CHS) = c_{pol}/c_{aq} \qquad (17)$$

where $c_{pol}$ and $c_{aq}$ are the analyte concentration in the silicone polymer and in the aqueous phase, respectively.

A low water solubility and a low boiling point of the observed substances lead to a high $K_D$ value.[28] Distribution coefficients for chlorinated hydrocarbons in the polydimethylsiloxane/water system have been measured by Zimmermann et al.[27] At 25°C the following values have been determined: $K_D(CH_2Cl_2) = 11$; $K_D(CHCl_3) = 41$; and $K_D(CHCl=CCl_2) = 245$. Hence, for aqueous solutions of identical concentration the molar concentrations $c_{pol}$ of the chlorinated hydrocarbons in the cladding are quite different. The expected molar concentration ratios in the silicone polymer, calculated from the $K_D$ values, should be $c(CH_2Cl_2)/c(CHCl_3) \approx 1:4$ and $c(CH_2Cl_2)/c(CHCl=CCl_2) \approx 1:22$. Assuming that only the pseudo-Beer's term (first term of Eq. 7) describes the interdependence of CHS absorbance and concentration values and assuming further that the molar extinction coefficient is similar for all compounds in the silicone, these concentration

ratios should correspond to the ratios of the slopes of the calibration curves. From the curves in Fig. 5, plotted for low analyte concentrations, where the RI influence on the absorbance signal is small, the following ratios of sensitivities $m(CHS)$ at corresponding wavelengths have been determined: $m(CH_2Cl_2)/m(CHCl_3) \approx 1:5$ at 1692 nm and $m(CH_2Cl_2)/m(CHCl=CCl_2) \approx 1:35$ at 1650 nm. These ratios were obtained from a regression of the absorbance/concentration data in the linear part of the calibration curves (concentration values up to 0.094 mol
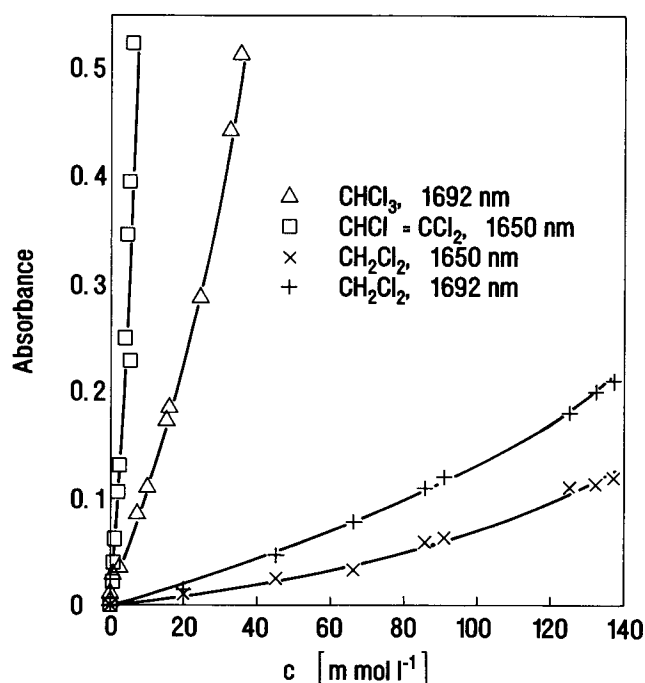


FIG. 5. Evanescent field absorbance signal of a 6.43-m length/230-$\mu$m cladding/210-$\mu$m core fiber sensor vs. molar analyte concentration in the aqueous phase for $CH_2Cl_2$, $CHCl_3$, and $CHCl=CCl_2$ at wavelengths of 1650 nm and 1692 nm.
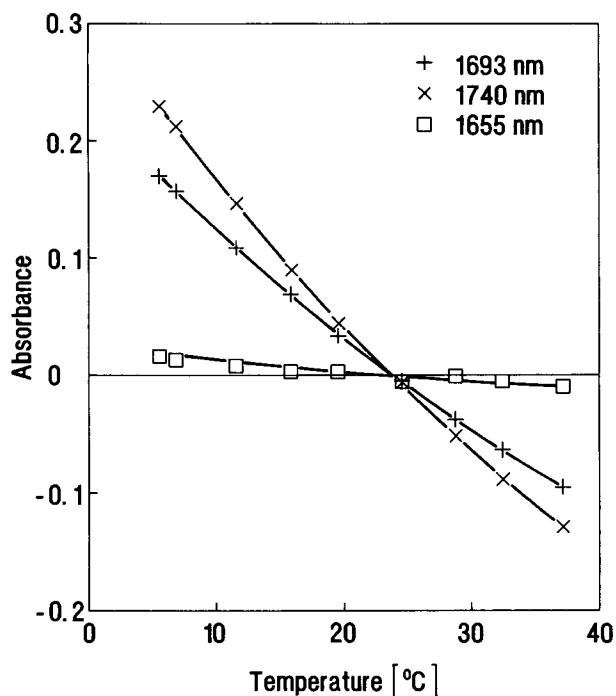
FIG. 6. Temperature dependence of the sensor signal at wavelengths of 1655, 1693, and 1740 nm; 6.43-m length/500-$\mu$m cladding/400-$\mu$m core fiber sensor in pure deionized water.



FIG. 7. Absorbance signal of a 500-$\mu$m cladding/400-$\mu$m core fiber sensor vs. molar CHCl=CCl$_2$ concentration for several fiber lengths.

L$^{-1}$ for dichloromethane, 0.029 mol L$^{-1}$ for chloroform, and 0.0023 mol L$^{-1}$ for trichloroethylene were used). The data match—at least qualitatively—with the values predicted by the distribution coefficients. It is obvious that this comparison can only be an approximation. On the one hand, the molar extinction coefficients of the compounds are not equal and, on the other hand, the RI influence on the sensor response signal cannot be neglected. Looking at Eq. 7, a strong dependence of RI on the effective absorptivity and the refraction term can be stated and has already been shown in Figs. 1 and 2. If dichloromethane (RI = 1.4246) is enriched, the "mixed" refractive index of the cladding (polymer plus analyte) decreases, which leads to lower absorbance values. If chloroform (RI = 1.4459) is enriched in the cladding, a higher absorbance will be obtained due to the increase in RI around the fiber core. For trichloroethylene (RI = 1.4774) this effect is still stronger, and for high concentrations the RI of the cladding exceeds the RI of the core and light will be completely coupled out from the fiber, resulting in an infinite absorbance signal. The discrepancies between the ratios of the CHS sensitivities and the ratios predicted from the $K_D$ values are caused mainly by the discussed deviations in the molar extinction coefficients and the RI effects on the sensor signal during analyte enrichment in the cladding.

The effect of the change in RI at several wavelengths can be shown by observing the temperature dependence of the sensor signal. Figure 6 shows the changes in absorbance of a sensor (reference temperature 25.5°C) which has been thermostated in pure deionized water. With application of increasingly higher temperatures, the cladding swells and the density of the polysiloxane decreases. Due to this factor, both terms in Eq. 7 diminish and negative absorbance values are obtained. If the tem-
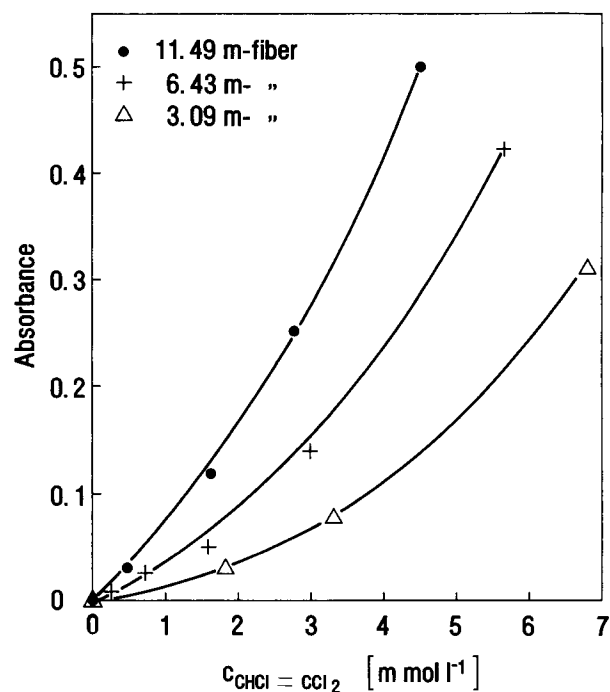
perature is decreased to values below 25.5°C, these effects are reversed and a positive absorbance offset can be observed. The second term of Eq. 7 corresponds to the signal at a nonabsorbing wavelength of the polysiloxane, while at an absorbing wavelength the contribution of the first term becomes more important. Looking at a weakly absorbing wavelength of the cladding at 1655 nm (the attenuation spectrum of the polydimethylsiloxane-clad fiber is shown in a preceding report),[9] one finds that temperature variations lead only to minor changes in the absorbance signal. At 1740 nm the cladding exhibits higher values of light attenuation due to a higher contribution of the first term in Eq. 7, and a steeper curve is obtained. At 1692 nm the cladding absorption of light reaches a maximum, which leads to the highest influence of RI on the sensor response. Going from wavelengths of low to wavelengths of high polymer absorption, temperature influences on the sensor signal become more and more distinct. Hence, if temperature deviations between reference and sample measurement occur, a nonlinear baseline offset can be expected that could lead to drastic changes in the peak shape. This influence has to be considered, especially for low analyte concentrations in the aqueous solution.

The dependence of the sensor absorbance signal on the fiber length can be seen from Fig. 7, where the absorbance/concentration values for trichloroethylene are plotted for several fiber lengths. Because of the high refractive index of this chlorinated hydrocarbon, a strong positive deviation from linearity can be observed (see also the Theory section). In spite of the bending of the curves, the signal is proportional to the fiber length for identical analyte concentrations. For none of the curves is a remarkable baseline offset due to the second term of Eq. 7 obtained. This result has also been found for
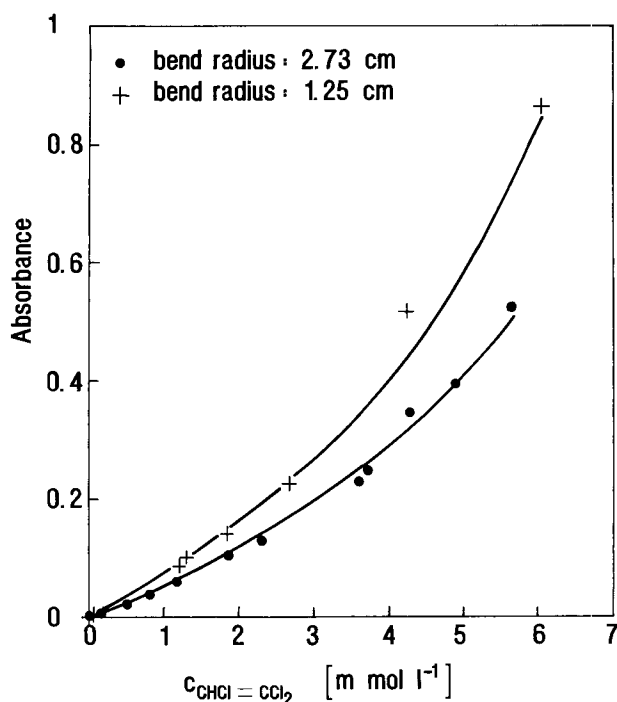
FIG. 8. Absorbance signal of a 6.43-m length/500-$\mu$m cladding/400-$\mu$m core fiber sensor for several bend radii.
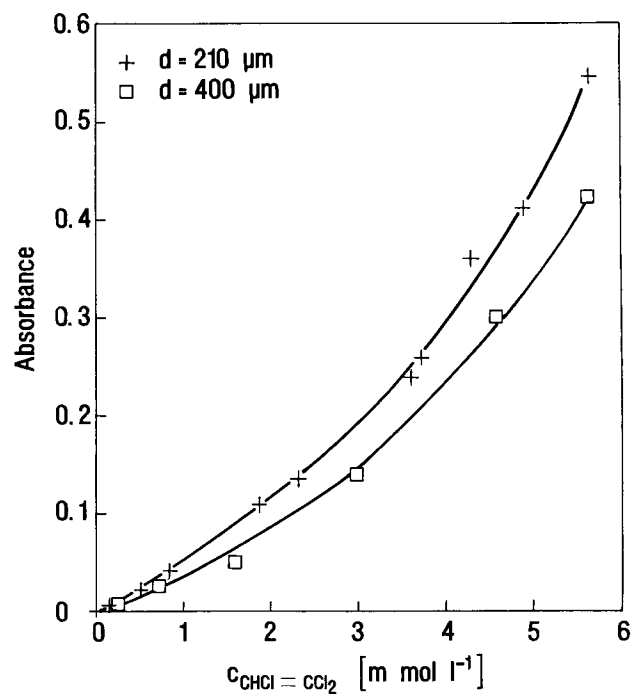


FIG. 9. Absorbance signal of a 6.43-m length sensor for several fiber core diameters.

dichloromethane and chloroform. According to Eq. 7, the contribution to the absorbance of the first term is linearly correlated to the fiber length, while the second term (which adds a constant absorbance value to the total absorption signal) is not influenced by this parameter. From these observations it can be deduced that the absorbance signal of the measured substances is given mainly by the "pseudo-Beer's-term" of Eq. 7, while the contribution of the refraction term seems to be negligible. Otherwise, no proportionality of EFAS signal and fiber length should appear.

As mentioned in the theoretical section, the bend radius $R$ of the fiber coil is another important parameter influencing the signal of an evanescent wave sensor. A signal enhancement with smaller bend radius was confirmed for all three chlorinated hydrocarbons and can be seen for trichloroethylene enrichment in Fig. 8. This result is due to the reordering of the optical modes when the waveguide is bent, and it was already observed by DeGrandpre and Burgess.[29]

The influence of the fiber diameter on the sensor signal has been tested as a final parameter. For a thicker fiber diameter the light has to pass longer distances in the glass core between two points of internal reflection. From simple trigonometric considerations, one can conclude that the number of reflections increases with decreasing fiber diameter. The resulting absorbance signal is shown in Fig. 9, where the response of two sensors with identical geometries but different fiber diameters is plotted against the concentration of trichloroethylene. In the case of dichloromethane and chloroform the same effect has been found qualitatively.

For an unbent fiber the absorbance should be inversely proportional to the fiber radius $r$ (compare Eqs. 7 and 8). When the optical cable is bent, the light-transmitting

part of the fiber cross section decreases (see Table I). Only light rays entering the curved part of the fiber at the outer diameter are transported by total reflection,[18] while light rays entering at the inner diameter are refracted into the surrounding medium. Due to this transport of light only at the outer part of the bent fiber, the inner part of the fiber stays "dark" if coils of relatively small bend radii are achieved. This "dark" fiber part has no influence on the signal. In the case of bent fibers with sufficiently small values of $R$, the total reflection areas at the outer parts of a thick and a thin fiber are not proportional to the fiber diameter. When comparing straight fibers of 210-$\mu$m core and 400-$\mu$m core, one would expect a 1.9-fold increase in the absorption values. However, due to the effects discussed, only a 1.3-fold enhancement can be noted from Fig. 9 in the case of bent fibers.

**Kinetics and Diffusion.** Kinetics experiments have been performed by measuring the CHS absorbance values vs. the time. Typical data have already been presented in a preceding paper.[9] For $CHCl_3$ the resulting $t_{90}$ values are shown in Fig. 10 for a 6.43-m sensor (500-$\mu$m-o.d. cladding/400-$\mu$m-o.d. core fiber) as a function of the analyte concentration for stirred and unstirred solutions. The response times decrease by a factor of $\approx 7$ when the solutions are stirred. This observation clearly indicates that the molecular movement through the Nernstian boundary layer should be the rate-determining step, because stirring cannot change the diffusion behavior in the polymer bulk. The shape of the curve for an unstirred solution is quite similar to that of a stirred solution, indicating in both cases an increase in the $t_{90}$ values with the concentration.

The mechanism of diffusion can be determined by applying the second Fickian law on the kinetics data for
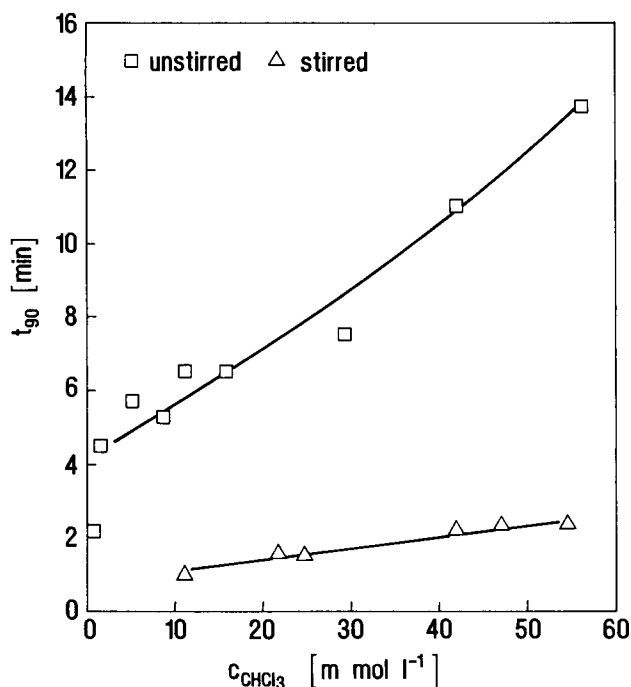
FIG. 10. $t_{90}$ values of a 6.43-m length/500-$\mu$m cladding/400-$\mu$m core fiber sensor vs. molar $CHCl_3$ concentration for stirred and unstirred solutions.



FIG. 11. $\ln(1 - c(t)/c_e)$ values of a 210-$\mu$m core and 400-$\mu$m core fiber sensor for several $CHCl_3$ concentrations.

CHS enrichment. As mentioned above, Eq. 13 cannot be solved if the rate determination is influenced by both the diffusion through the aqueous boundary layer and the diffusion through the polysiloxane matrix. But if the system does not show an influence of molecule movement through the NBL, it should be described by non-steady-state gel diffusion in the polymer bulk. In this case, for short enrichment times (with an initial analyte concentration $c(t = 0) = 0$) the solution of Eq. 13 can be approximated by:

$$c(t)/c_e = k_1 \cdot t^{1/2} \tag{18}$$

where $c(t)$ is the concentration at time $t$, $c_e$ is the concentration when the equilibrium is reached, and $k_1$ is a constant containing information about the diffusion coefficient of the analyte, the diameters of the hollow cylinder, and the sensor geometry.[24]

If the system, on the other hand, is described by a film diffusion in the Nernstian boundary layer, the solution of Eq. 13 for steady-state conditions can be approximated by:

$$\ln(1 - c(t)/c_e) = -k_2 \cdot t \tag{19}$$

where $k_2$ is a constant containing information similar to that in $k_1$.[24]

The $CHCl_3$ absorbance signal of the sensor shows only slight deviations from linearity (cf. Fig. 5). Hence, the time-dependent absorbance data are linearly correlated to the corresponding concentrations:

$$c(t)/c_e = A(t)/A_e \tag{20}$$

where $A(t)$ is the absorbance at time $t$ and $A_e$ is the absorbance when the equilibrium is reached.

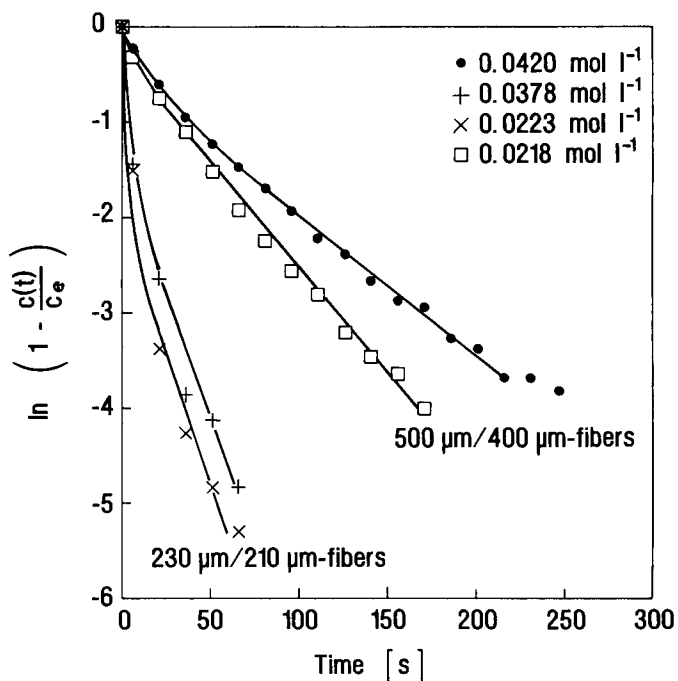Sensor data for chloroform in stirred solutions have been evaluated by using Eqs. 19 and 20. In Fig. 11 some

of the obtained $\ln(1 - c(t)/c_e)$ values are plotted against $t$. Generally, after induction periods of up to 10 s for the 230-$\mu$m-o.d.-clad fiber and 10 to 30 s for the 500-$\mu$m-o.d.-clad fiber, a linear relationship can be observed over a wide range. Due to this dependence, the uptake of $CHCl_3$ by the cladding seems to be described mainly by steady-state film diffusion. No remarkable influence of molecule movement in the polymer bulk is observed.

The following properties have to be fulfilled to see steady-state film diffusion during CHS enrichment: The analyte concentrations at the interfaces of solution/NBL and NBL/polymer (cf. points A and B in Fig. 3) have to be constant over time. The concentration at point A is constant due to a fast molecule transport by convection in the aqueous solution. The analyte concentration at point B, on the other hand, stays at a relatively low and constant value due to a fast diffusion rate in the polymer bulk (the "liquid-like" structure of the polysiloxane already discussed above allows this fast transport of the chloroform molecules). Hence, if the Nernstian postulate of a constant extension $\delta_N$ of the NBL under similar hydrodynamic conditions is fulfilled, the concentration gradient $\Delta c/\delta_N$ should be constant over time (cf. Eq. 15) and steady-state diffusion is observed.

Moreover, the thickness of the two fiber claddings of 10 $\mu$m and 50 $\mu$m, respectively, is small compared to the thickness of the diffusion layer, which is typically in the range of 100 to 1000 $\mu$m.[30] So, if the analyte diffusion coefficients in water and in the polydimethylsiloxane matrix are in the same range, the contribution of gel diffusion to the uptake should be very small.

The kinetics data from Fig. 10 show an increase in the $t_{90}$ values with increasing $CHCl_3$ concentrations. This increase in the sensor response times indicates that the gradient $\Delta c/\delta_N$ grows slower than the number of analyte molecules in the aqueous solution. Therefore, in contrast

to the assumptions made in the theoretical section, the increase in analyte flux is not proportional to the concentration $c_\infty$ (cf. Eq. 15).

One possible explanation of this behavior could be an increase in the analyte concentration $c_s$ at the sensor surface with increasing $c_\infty$. In dilute CHS solutions only a small number of molecules arrive at the polymer membrane per unit of time and, therefore, the surface concentration is quite low. Hence, if $c_s \approx 0$, $\Delta c$ is approximately given by the value of the analyte concentration in the solution $c_\infty$ (cf. Eq. 16).

At higher analyte concentrations in the aqueous solution, higher surface concentrations at the polysiloxane cladding could be expected (caused by a higher degree of "occupation" of the sensor surface with CHS molecules). In this case $\Delta c$ is significantly smaller than $c_\infty$, which means that the gradient $\Delta c / \delta_N$ does not grow to the same extent as the $CHCl_3$ concentration. As a result, at these concentrations higher $t_{90}$ values are obtained.

Another possible explanation of this behavior could be a stronger deviation of the real concentration profile from the idealization of the Nernstian boundary layer at higher CHS concentrations. The simplified model of Nernst substitutes the real differential quotient $dc/dx$ from Eq. 14 by the constant difference quotient $\Delta c / \delta_N$. However, with higher analyte concentrations, the real concentration profile compared to the approximation of the NBL should expand much more into the solution, leading to an effectively higher thickness of the diffusion layer. So, at higher concentrations the slope of the real gradient $dc/dx$ is flattened in comparison to the ideal $\Delta c / \delta_N$, resulting in longer response times.

Also other explanations for the increase in the $t_{90}$ values at higher concentrations are possible. The uptake of chloroform into the polysiloxane membrane could change the physical behavior of the cladding material, which could lead to a different molecule flux through the Nernstian boundary layer.

Kinetics measurements for $CH_2Cl_2$ and $CHCl=CCl_2$ have also been performed but are difficult to interpret. The data of dichloromethane are different from those obtained by measurements in chloroform solutions. Due to its low distribution coefficient, the sensor is almost equilibrated during the induction period before a stable concentration gradient can develop at the sensor surface. Hence, the $t_{90}$ values for stirred and unstirred solutions obtained with the 230-$\mu$m-o.d.-clad fiber sensor are quite identical.

The interpretation of the kinetics data for trichloroethylene is difficult, too. As can be seen in Fig. 7, the absorbance signal shows a strong deviation from linearity. Therefore, the sensor response cannot be linearly correlated to the concentration as assumed before (cf. Eq. 20), and no linear dependence is found when $\ln(1 - c(t)/c_e)$ is plotted against time.

## CONCLUSION

Up to now the number of kinetics measurements made with polymer clad evanescent wave absorbance sensors has not been remarkable.[31,32] Starting from the results discussed in this paper, faster-detecting EFAS sensors with response times of a few minutes for CHS can be built by using commercially available silicone-clad quartz glass fibers with an outer diameter $<230 \mu$m. By chemical "tailoring" of silicone membranes with higher distribution coefficients for the relevant analytes, the limits of detection can be decreased efficiently.

Further investigations have to be done to see the influence of temperature on the sensor signal during analyte enrichment. Temperature effects will influence, on the one hand, the distribution coefficient of the analyte in the water/polysiloxane system and, on the other hand, the RI of the cladding, leading to changes in the analyte signal. Moreover, the potential of EFAS sensor measurements can also be extended to other nonpolar organic water contaminants, e.g., aromatic compounds like benzene, toluene, and xylene.

For solutions containing more than one compound, resulting in strong overlapping of the EFAS absorbance spectra obtained, multivariate calibration methods like partial least-squares regression[33,34] have to be used.

1. H. Graf, GIT Fachz. Lab. **10**, 964 (1989).
2. S. M. Angel, Spectroscopy **2**, 38 (1987).
3. R. W. Seitz, CRC Crit. Rev. Anal. Chem. **19**, 135 (1988).
4. F. Goos and H. Hänchen, Ann. Physik **6**, No. 1, 333 (1947).
5. O. S. Wolfbeis, H. E. Posch, and H. W. Kroneis, Anal. Chem. **57**, 2556 (1985).
6. F. P.Milanovich, D. G. Garvis, S. M. Angel, S. M. Klainer, and L. Eccles, Anal. Inst. **15**, 137 (1986).
7. S. Simhony, A. Katzir, and E.-M. Kosower, Anal. Chem. **60**, 1908 (1988).
8. M. D. DeGrandpre and L. W. Burgess, Anal. Chem. **60**, 2582 (1988).
9. J. Bürck, J.-P. Conzen, and H.-J. Ache, Fresenius J. Anal. Chem. **342**, 394 (1992).
10. M. G. Voronkov, V. P. Mileshkevich, and Y. A. Yuzhelevskii, *The Siloxane Bond* (Consultants Bureau, New York, London, 1974), p. 31.
11. *Handbook of Chemistry and Physics*, R. C. Weast, Ed. (CRC Press, Boca Raton, Florida, 1977/78), 58th ed., p. E-56.
12. N. J. Harrick, *Internal Reflection Spectroscopy* (Harrick Scientific, Ossining, New York, 1979), pp. 30–33.
13. L. C. Bobb, H. D. Krumboldt, and J. P. Davis, SPIE Proc. Chem. Biochem. Environ. Appli. Fibers **990**, 164 (1988).
14. N. J. Harrick, *Internal Reflection Spectroscopy* (Harrick Scientific, Ossining, New York, 1979), pp. 19–25.
15. M. D. DeGrandpre and L. W. Burgess, Appl. Spectrosc. **44**, 273 (1990).
16. D. Gloge, Appl. Opt. **10**, 2252 (1971).
17. T. B. Colin, K.-H. Yang, and W. C. Stwalley, Appl. Spectrosc. **45**, 1291 (1991).
18. T. Takeo and H. Hattori, Japan. J. Appl. Phys. **21**, 1509 (1982).
19. *Müller-Pouillets Lehrbuch der Physik*, A. Eucken, O. Lummer, and E. Waetzmann, Eds. (Vieweg und Sohn, Braunschweig, 1929), 11th ed., Vol. 2, Optik, pp. 1639–1642.
20. W. Vielstich, Z. Elektrochem. **57**, 646 (1953).
21. W. Hayduk and H. Laudie, AIChE J. **20**, 611 (1974).
22. F. Helfferich, *Ionenaustauscher* (Verlag Chemie, Weinheim, 1959), Vol. 1, p. 316.
23. *Silicon-Based Polymer Science*, J. M. Zeigler and F. W. G. Fearson Eds. (American Chemical Society, Washington, D.C., 1990), pp. 47–68.
24. J. Crank, *Mathematics of Diffusion* (Clarendon Press, Oxford, 1955), 2nd ed., Chap. 5, pp. 69–88.
25. F. Helfferich, *Ionenaustauscher* (Verlag Chemie, Weinheim, 1959), Vol. 1, pp. 244–251.
26. L. G. Weyer, Appl. Spectrosc. Reviews **21**, 1 (1985).

27. B. Zimmermann, J. Bürck, and H.-J. Ache, KfK Report No. 4967 (Kernforschungszentrum Karlsruhe GmbH, 1991), pp. 43–49.
28. R. Wyzgol, *Zur Optimierung der Bestimmung organischer Stoffe in Luft und Wasser mit Hilfe der Infrarotanalyse extrahierender Membranen,* Doctoral thesis, Universität Essen (1989), pp. 89–93.
29. M. D. DeGrandpre and L. W. Burgess, ISA Trans. **28,** No. 2, 71 (1988).
30. W. R. A. Vauck and H. A. Müller, *Grundoperationen chemischer Verfahrenstechnik,* (Verlag Chemie, Weinheim, 1988), 7th ed., p. 527.
31. L. L. Blyler, Jr., R. A. Lieberman, L. G. Cohen, J. A. Ferrara, and J. B. MacChesney, Poly. Eng. Sci. **29,** 1215 (1989).
32. C. L. Arthur and J. Pawliszyn, Anal. Chem. **62,** 2145 (1990).
33. K. R. Beebe and B. R. Kowalski, Anal. Chem. **59,** 1007 (1987).
34. P. Geladi and B. R. Kowalski, Anali. Chimi. Acta **185,** 1 (1986).